nature COMMUNICATIONS

ARTICLE

Received 17 Sep 2014 | Accepted 27 Mar 2015 | Published 7 May 2015

DOI: 10.1038/ncomms8069

Subwavelength-thick lenses with high numerical apertures and large efficiency based on high-contrast transmitarrays

Amir Arbabi[1], Yu Horie[1], Alexander J. Ball[1], Mahmood Bagheri[2] & Andrei Faraon[1]

Flat optical devices thinner than a wavelength promise to replace conventional free-space components for wavefront and polarization control. Transmissive flat lenses are particularly interesting for applications in imaging and on-chip optoelectronic integration. Several designs based on plasmonic metasurfaces, high-contrast transmitarrays and gratings have been recently implemented but have not provided a performance comparable to conventional curved lenses. Here we report polarization-insensitive, micron-thick, high-contrast transmitarray micro-lenses with focal spots as small as 0.57λ. The measured focusing efficiency is up to 82%. A rigorous method for ultrathin lens design, and the trade-off between high efficiency and small spot size (or large numerical aperture) are discussed. The micro-lenses, composed of silicon nano-posts on glass, are fabricated in one lithographic step that could be performed with high-throughput photo or nanoimprint lithography, thus enabling widespread adoption.

[1] T. J. Watson Laboratory of Applied Physics, California Institute of Technology, 1200 E California Blvd., Pasadena, California 91125, USA. [2] Jet Propulsion Laboratory, California Institute of Technology, Pasadena, California 91109, USA. Correspondence and requests for materials should be addressed to A.F. (email: faraon@caltech.edu).

Flat lenses are most commonly realized with Fresnel structures. However, geometrical complexity of Fresnel lenses and the low efficiency of Fresnel zone plates make them not well suited for integration with wafer-scale processing. Effective medium structures have been proposed as an alternative[1–5], but their deep subwavelength structures and high aspect ratios make their fabrication challenging. Recently, diffractive elements based on plasmonic metasurfaces composed of 2D arrays of ultrathin scatterers have attracted significant attention[6–14], but their efficiency is limited to 25% by fundamental limitations[15,16] and they also suffer from material absorption[11].

A novel approach is to use high-contrast gratings (HCGs), fabricated from semiconductors or high refractive index (high-index) dielectrics[17–19], that can be designed with large reflection[20] or transmission[21] efficiencies. Wavefront control was originally achieved by rendering one dimensional gratings aperiodic by gradually modifying the local period and duty cycle of the grating[21–23]. Reflective focusing mirrors were realized using this approach[21,23,24]. Most devices based on 1D HCGs work only with one linear polarization and operate based on phase accumulation through the propagation or low-quality factor resonances in the grating. More recently, half wave plates were implemented using thin 1D HCGs, and lenses were realized through the Pancharatnam–Berry phase by locally rotating the half wave plates[25]. The later devices (which are referred to as dielectric gradient metasurface lenses) should be illuminated with a circularly polarized light, and their output is cross-polarized with respect to the input light[25].

A promising class of aperiodic HCGs can be realized by positioning high-index dielectric scatterers on a periodic subwavelength 2D lattice. The high-index results in negligible interaction among the scatterers, so the light scattered at each lattice site is dominated by the scatterer proprieties rather than by the collective behaviour of multiple coupled scatterers in the lattice. We refer to high-contrast zero-order gratings composed of disconnected scatterers, which operate in this local scattering regime, as high-contrast arrays. The term high-contrast transmitarrays (HCTAs) is used when they are designed for large transmission. Low numerical aperture (NA) lenses based on HCTA have been recently reported[26,27].

Here we explain the HCTA concept and discuss its unique features resulting from the localized scattering phenomena, which enable the implementation of diffractive elements with rapidly varying phase profiles. To demonstrate the HCTA versatility, we present design, simulation, fabrication and characterization results of polarization-insensitive high-NA micro-lenses with high focusing efficacy. High-NA lenses are required in microscopy, high-density data recording, focal plane arrays and coupling between on-chip photonic components and free-space beams. Current techniques to fabricate on-chip devices that impose rapid phase variation require grey-scale lithography[28,29], a process that is difficult to control. On the other hand, the HCTA devices provide a more reliable alternative with fabrication techniques that lend themselves to wafer-scale processing.

Results

Transmission characteristics of periodic HCTAs. An array of circular amorphous silicon posts arranged on a hexagonal lattice with subwavelength lattice constant is shown schematically in Fig. 1a. Due to the subwavelength lattice constant, the array acts as a zeroth order grating, and it is completely described by its transmission and reflection coefficients. Figure 1b shows the simulated transmission and phase of the transmission coefficient for two gratings composed of circular amorphous silicon posts arranged in hexagonal and rectangular lattices, as functions of lattice constant and post diameter (see Fig. 1 legend for dimensions). The gratings are designed to operate at $\lambda = 1{,}550$ nm, but the concept is scalable to any wavelength. In each case, the amplitude and phase depend primarily on the post diameter, which is an indication that, in this parameter regime, the scattering is a local effect and is not affected significantly by the coupling among the scatterers. This is also confirmed by the almost identical transmission properties of the hexagonal and square lattices. Examining the near-field distribution of the grating reveals the underlying physical mechanism behind the local scattering effect. As shown in Fig. 1c, light is concentrated inside the posts that behave as weakly coupled low-quality factor resonators. This behaviour is fundamentally different from the low-contrast gratings operating in the effective medium regime whose diffractive characteristics are mainly determined by the duty cycle and the filling factor. We also note that the structures created by changing the bar width and period of 1D HCGs (refs 21,23,24) are not considered HCTA since there is a strong coupling along the bar direction, and rapid variations of the local transmission or reflection properties of the structure are not achievable along that direction.

Design of HCTA micro-lenses. To design an HCTA that implements a transmissive phase mask, we find a family of periodic HCTAs with the same lattice but with different scatterers that provide large transmission amplitudes while their phases span the entire 0 to 2π range. Such a family is shown in Fig. 1d where the diameters of 940-nm tall posts are varied from 200 to 550 nm in a hexagonal lattice with an 800-nm period while transmission is $>92\%$. Large transmission has been reported for an array of circular posts with a height of 220 nm (refs 30,31), but simulation results show that full 2π phase coverage cannot be achieved for such an array by only changing the in-plane geometrical parameters. To design an HCTA that implements a desired phase mask, we start from an empty lattice and sample the desired phase profile at the lattice sites. Then, at each lattice site, we place a scatterer from the periodic HCTAs that most closely imparts the desired phase change onto the transmitted light. Any arbitrary transmissive phase masks can be realized using this method. To minimize scattering from aperiodic HCTAs into non-zero orders, a gradual change in the scatterer size is preferable.

The unprecedented possibility to realize any transmissive masks using HCTAs enables the implementation of micro-lenses with exotic phase profiles, such as high-NA micro-lenses, which are optimized for specific tasks. To design these components, the conventional ray tracing technique is not applicable. A general rigorous technique for determining the optimum transmissive mask to shape an incident optical wavefront to a desired form is given in Supplementary Note 1. Using this technique and the HCTAs in Fig. 1d, we found the optimum phase masks for micro-lenses that focus $\lambda = 1{,}550$ nm light from a single-mode fibre to the smallest diffraction limited spots. We designed a set of 400-μm diameter high-NA micro-lenses that focus the light from a single-mode fibre located 600 μm away from the back side of a substrate (500-μm thick fused silica) to points located at distances ranging from $d = 50$ μm to $d = 500$ μm away from the micro-lenses (Fig. 2a). We refer to d as the focusing distance.

Micro-lens full-wave simulation results. The performance of the micro-lenses was evaluated by 3D finite difference time domain (FDTD) simulations[32]. To reduce the simulation size, micro-lenses with the same NA but with a factor of four smaller dimensions (100 μm diameter, 150 μm spacing between the

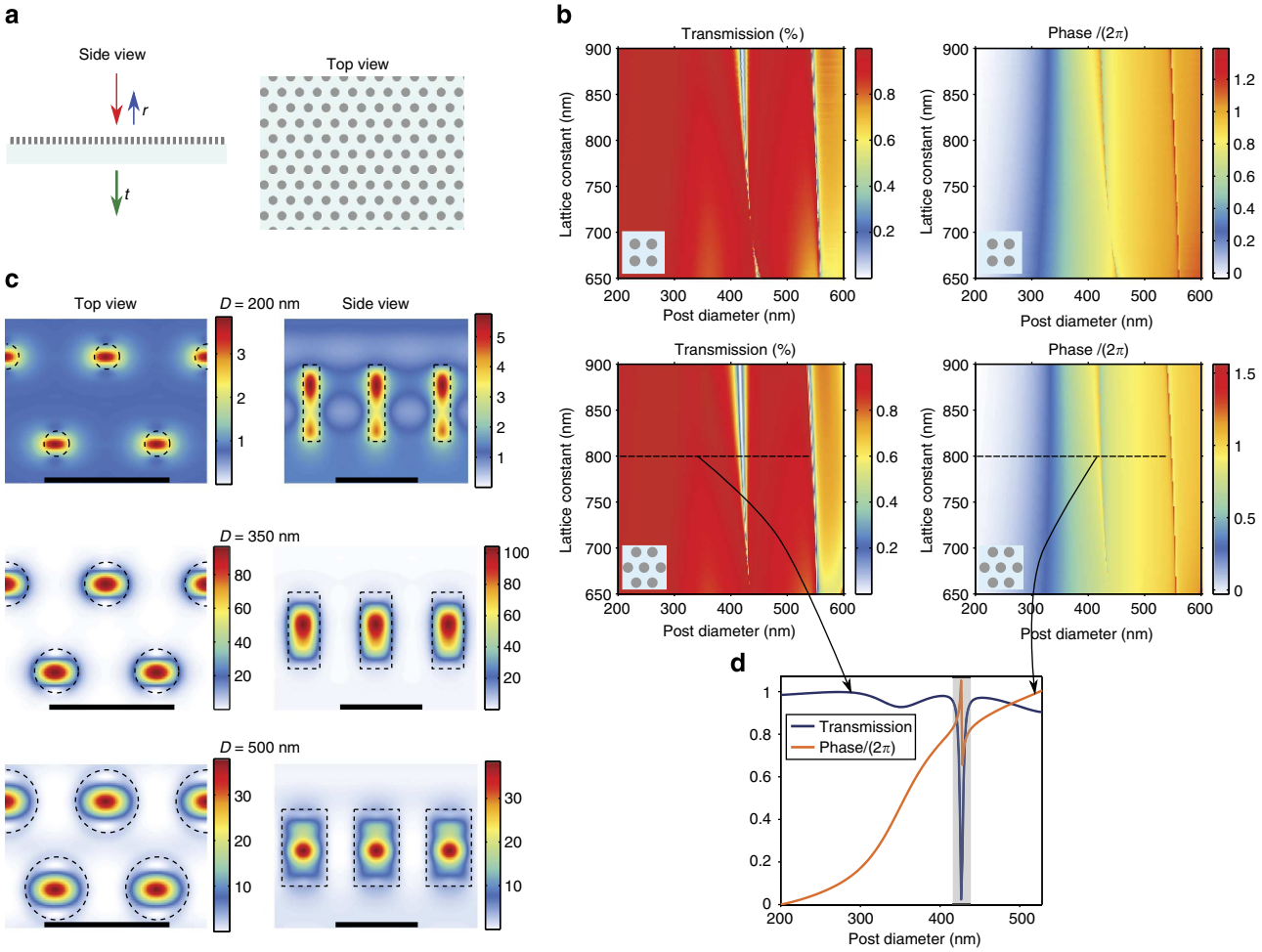

Figure 1 | Simulation results of periodic HCTAs. (**a**) A schematic representation of a periodic HCTA composed of high-index posts in a hexagonal lattice with transmission coefficient t and reflection coefficient r. The posts rest on a low-index substrate. (**b**) Simulated transmission and phase of the transmission coefficient for hexagonal and square lattice periodic HCTAs composed of circular amorphous silicon posts on a fused silica substrate as a function of the lattice constant and the post diameter. The insets show the corresponding lattices. (**c**) Top and side views of the colour coded magnetic energy density in a periodic HCTA for different post diameters D. The dashed black lines depict the boundaries of the silicon posts. A plane wave with magnetic energy density of 1 is normally incident on the silicon posts from the top. Scale bar, 1 μm. (**d**) Simulated transmission and phase of the transmission coefficient for a family of periodic hexagonal HCTAs with lattice constant of 800 nm, and varying post diameters. The shaded part of the graph is excluded when using this graph to map transmission phase to post diameter. In all these simulations, the posts are made of amorphous silicon ($n = 3.43$), are 940-nm tall and the wavelength is $\lambda = 1{,}550$ nm.

illuminating fibre and the back side of a 125-μm thick substrate) were simulated (see Methods for details). Figure 2b,c show the results for a micro-lens that focuses at $d = 25$ μm away from the lens. The full width at half maximum (FWHM) of the focal spot is 1.06 μm or 0.68λ ($\lambda = 1{,}550$ nm). To differentiate between the power transmitted through the lens and the power directed by the lens toward the focus, we define the focusing efficiency as the fraction of the incident light that passes through a circular aperture in the plane of focus with a radius equal to three times the FWHM spot size. The simulation indicates 85% transmission efficiency and 72% focusing efficiency for the lens shown in Fig. 2b,c.

Simulated values of the transmission, focusing efficiency and FWHM spot size for several micro-lenses with d ranging from 12.5 to 125 μm are presented in Fig. 2d. Higher NAs and smaller spot sizes correlate with decreased transmission and lower focusing efficiencies. This is due to the undersampling of the phase profiles of high-NA lenses, which rapidly vary close to the lens circumference. Shrinking the lattice constant of the HCTA reduces this trade-off (see Supplementary Note 2). The micro-lens with $d = 12.5$ μm has an FWHM spot size of 0.51 λ, which is close to the smallest possible diffraction limited value of 0.5 λ. The relatively high efficiency (>50%) and the diffraction limited focusing of this micro-lens confirms the validity of our technique for determining the optimum phase profile, and demonstrates an example of the high performance that can be achieved by HCTA flat diffractive elements.

Fabrication and characterization of micro-lenses. The high-NA lenses were fabricated in a hydrogenated amorphous silicon film deposited on a 500-μm thick fused silica substrate as described in the Methods section. A schematic illustration and images of the fabricated devices are shown in Fig. 3a–d. The characterization was performed in a setup (Fig. 4a) consisting of a custom built microscope that images the plane of focus of the micro-lens (see Methods). The micro-lenses were illuminated with 1,550-nm light emitted from a cleaved single-mode fibre positioned 600 μm away from the substrate back side. The normalized measured intensity profile at the plane of focus for a micro-lens with the focusing distance of $d = 50$ μm is shown in Fig. 4b. The intensity profiles

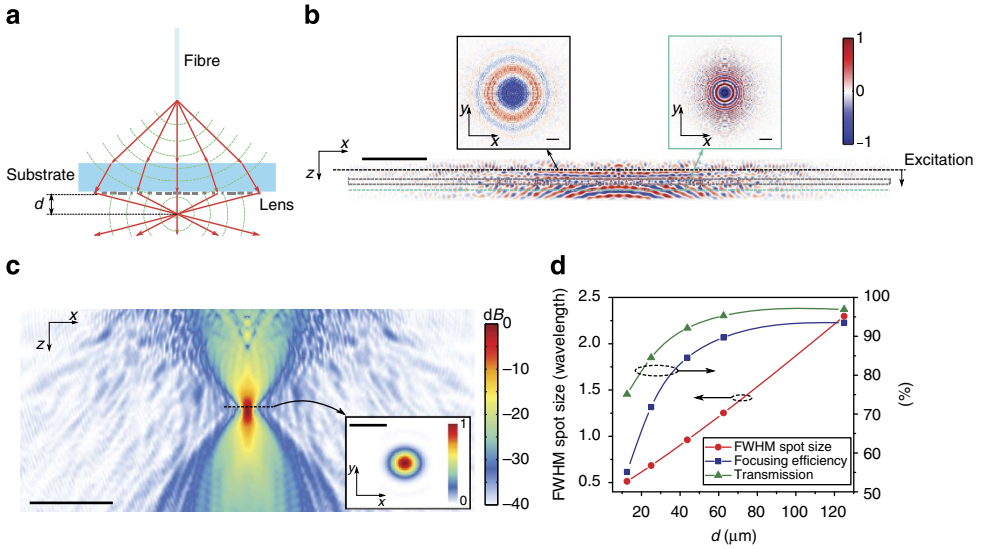

Figure 2 | Simulation results of high-NA HCTA micro-lenses. (**a**) Illustration of high-NA focusing of the light from a cleaved optical fibre using an HCTA micro-lens. (**b**) Electric field distribution at the *xz* cross section, in the excitation plane (inset), and immediately after passing through the micro-lens (inset). Incident light propagates along the *z* direction. Scale bars, 10 μm. (**c**) Logarithmic scale electric energy density in the *xz* cross section. The inset shows the real part of the *z* component of the Poynting vector at the plane of focus. Scale bars, 20 μm in the main figure and 2 μm in the inset. (**d**) Simulated plane of focus FWHM spot size, transmission and focusing efficiency of the high-NA HCTA micro-lenses for devices with varying focusing distances. The simulated points are shown by the symbols and the solid lines are eye guides. All the devices simulated in this figure are a factor of four smaller than the devices fabricated and measured in Figs 3 and 4.

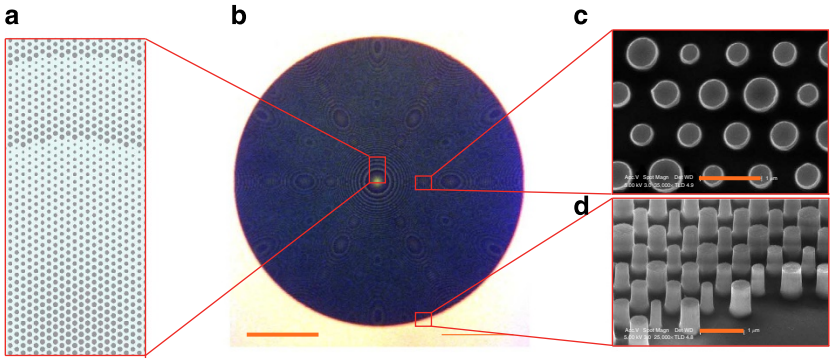

Figure 3 | Schematic illustration and images of fabricated HCTA lenses. (**a**) Schematic of the aperiodic HCTA used to realize a high-NA micro-lens. (**b**) Optical microscope image of a fabricated HCTA lens with large NA. Scale bar, 100 μm. (**c**,**d**) Scanning electron microscope images of the silicon posts forming the HCTA micro-lens. Scale bars, 1 μm.

for micro-lenses with different focusing distance are plotted in Fig. 4c.

Figure 4d shows the measured FWHM spot size, transmission and focusing efficiency for devices with different focusing distances. The micro-lens designed for $d = 50\,\mu m$ focuses light to a 0.57λ FWHM spot size, and the micro-lens designed for $d = 500\,\mu m$ shows $>82\%$ focusing efficiency. These results agree well with the simulation results presented in Fig. 2d, although the measured focusing efficiencies are 10% smaller (3% is attributed to reflection from substrate backside interface and 7% to scattering by the random roughness of the etched silicon posts). As it was expected from the simulations (Fig. 2d), the measured focusing efficiency decreases as the NA increases.

Wavelength dependence of HCTA micro-lenses. The wavelength dependence of the FWHM spot size and focusing efficiency of a micro-lens with $d = 175\,\mu m$ are presented in Fig. 4e. The FWHM spot size increases slightly at shorter wavelength, and the focusing efficiency reduces by $\sim 5\%$ at 50 nm away from the design wavelength. Also, by changing the laser wavelength from 1,550 to 1,450 nm, the focusing distance changed from ~ 175 to $\sim 195\,\mu m$.

Discussion

Table 1 summarizes the performance parameters of some of the experimentally reported thin flat micro-lenses. The HCTA micro-lenses with focusing efficiencies up to 82%, and FWHM spot sizes down to 0.57λ, to the best of our knowledge, represent the best performance among any types of flat high-NA micro-lens experimentally reported so far. As discussed earlier, lenses with small focal spot size (or equivalently high NA) require rapidly varying phase profiles and accurate correction for spherical aberration. Rapidly varying phase profiles can be realized using arrays of scatterers provided that the phase profile is sampled by the scatterers with sufficient spatial resolution, and the scatterers are weakly coupled to each other to avoid the strong near-field coupling among them, which filters the rapid spatial variations in the phase profiles. As we showed, the couplings among the scatterers are weak in the HCTA platform, and the array period is smaller than a wavelength; therefore, this platform allows for the

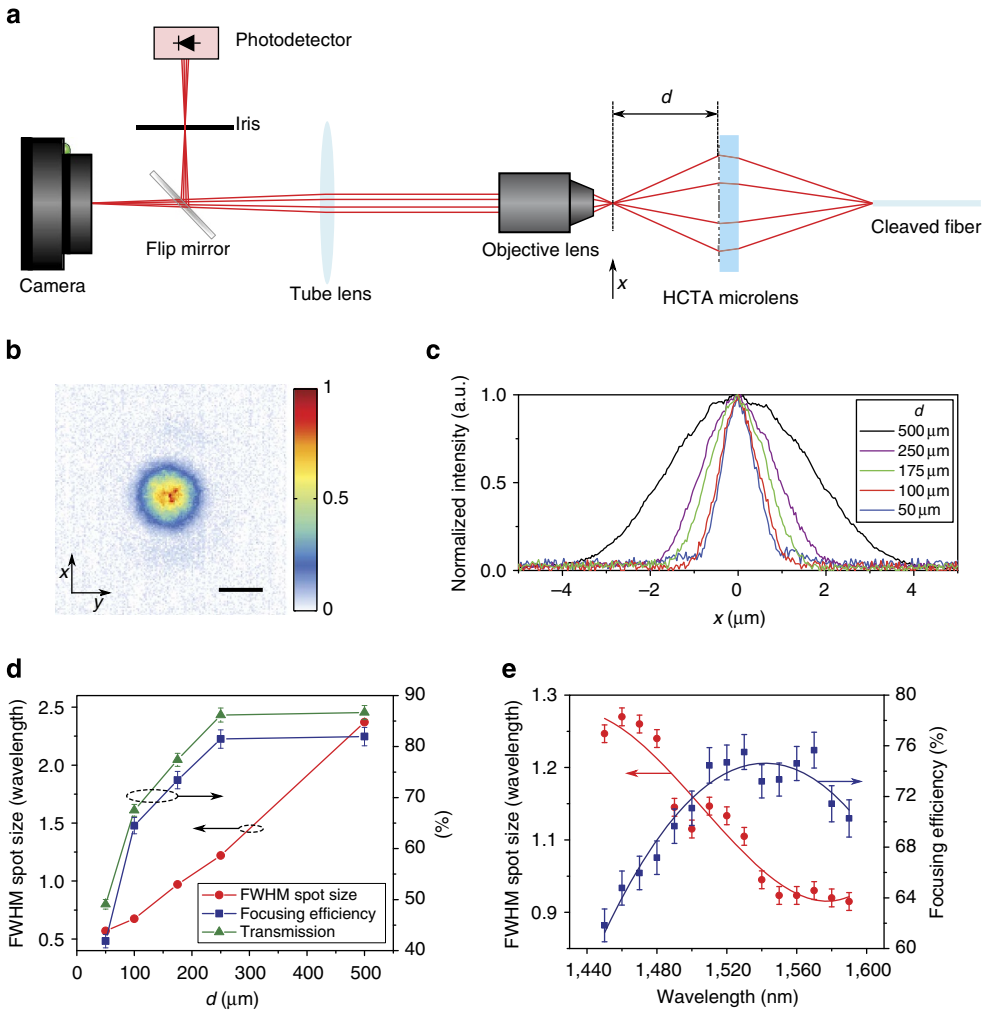

Figure 4 | Measurement results of high-NA HCTA micro-lenses. (**a**) Measurement setup for imaging the focal spot size and measuring the efficiency of the high-NA HCTA micro-lenses. The flip mirror was inserted into the setup only during efficiency measurements. (**b**) Measured 2D intensity profile at the plane of focus for a micro-lens with $d = 50\,\mu m$. Scale bar, $1\,\mu m$. (**c**) Normalized measured intensity profiles of high-NA micro-lenses with different focal lengths at their planes of focus. (**d**) Measured plane of focus FWHM spot size, transmission and focusing efficiency of the HCTA micro-lenses as a function of their focusing distance. (**e**) Wavelength dependence of the FWHM spot size, transmission and focusing efficiency for the micro-lens with $d = 175\,\mu m$. The measurement data in **d** and **e** are represented by the symbols, the solid lines are eye guides, and the error bars represent the s.d. for three alignment repetitions.

Table 1 | Summary of previously reported thin flat micro-lenses.

Reference	FWHM spot size (λ)	Efficiency	Polarization	λ (nm)	Lens thickness (λ)
Aieta *et al.*[11]	~33	~1%	Linear (cross*)	1,550	0.038
Ni *et al.*[12]	0.93	~10%†	Linear (cross)	676	0.044
This work	2.4	~82%	Insensitive	1,550	0.65
This work	0.57	~42%	Insensitive	1,550	0.65
Vo *et al.*[27]	~10	~70%	Insensitive	850	0.56
Lin *et al.*[25]	1.2	Not reported‡	Circular (cross)	550	0.18

*Cross: focused light is cross-polarized compared with the incident light.
†The ratio between the power of the cross-polarized light transmitted through the lens and the total power collected by the lens at the illumination side.
‡~45% diffraction efficiency is reported for a blazed grating at 550 nm, the operation wavelength of the lens. Higher diffraction efficiencies up to 85% can be theoretically achieved at other wavelengths. The diffraction efficiency is defined as the ratio of the first diffraction order power to the summation of the powers of the zeroth and first diffraction orders, and it does not take into account the losses due to reflection, absorption and incomplete polarization conversion.

implementation of high-NA lenses. Also, the rigorous method we used for finding the optimum phase profile for the lenses minimizes the spherical aberration. Any metasurface platform that achieves the 2π phase coverage, and samples rapidly varying phase profiles with subwavelength spatial resolution using weakly coupled scatterers can be used to implement the high-NA lenses; however, for achieving high focusing efficiency, it is essential to avoid platforms whose efficiencies are limited by absorption losses or fundamental physical limits.

In conclusion, the HCTAs enable shaping of the wavefront of light at will, efficiently and with subwavelength resolution. The exceptional freedom provided in the implementation of any

desired masks allows for achieving the best performance for any particular functionality. Combined with their planar form factor, these structures will enable on-chip optical systems created by cascading multiple diffractive elements. One recent demonstration is a planar retroreflector integrating an HCTA lens and a reflectarray focusing mirror[33]. We envision near-future application of HCTA-based devices in realization of more complex optical systems with new functionalities.

Methods

Sample fabrication. The HCTA pattern was defined in ZEP520A positive resist using a Vistec EBPG5000+ electron beam lithography system. After developing the resist, the pattern was transferred into a 70-nm thick aluminium oxide layer deposited by electron beam evaporation using the lift-off technique. The patterned aluminium oxide served as hard mask for the dry etching of the 940-nm thick silicon layer in a mixture of C_4F_8 and SF_6 plasma, and was subsequently removed through wet etching in a mixture of ammonium hydroxide and hydrogen peroxide at 80 °C.

Measurement procedure. The microscope uses a 100 × objective (Olympus UMPlanFl) with the NA of 0.95 and a tube lens (Thorlabs LB1945-C) with focal distance of 20 cm, which is anti-reflection coated for the 1,050–1,620 nm wavelength range. The magnification of the microscope was found by imaging a calibration sample with known feature dimensions.

The transmission and focusing efficiency of the micro-lenses were measured by inserting a flip mirror (as shown in Fig. 4a) in front of the camera. To measure the optical power focused by the micro-lens, the active area of the photodetector (Newport 818-IR) was reduced using an iris. The radius of the iris aperture was adjusted to three times of the measured FWHM spot size of the micro-lens on the camera. The total transmitted power was measured by opening the iris aperture completely. The total power incident on the microlens was measured by removing the micro-lens from the setup and bringing the fibre tip into the focus of the microscope. The non-uniformities seen in the intensity profile in Fig. 4 are due to the local variations in the sensitivity of the camera (Digital CamIR 1,550 by Applied Scintillation Technologies) and are observed even when directly imaging the light from an optical fibre.

Simulations. We found the electric and magnetic fields of the light from the fibre on a plane close to the lens using the plane wave expansion technique. Then, these fields were used to determine the equivalent electric and magnetic surface current densities, which were used as excitation sources in the FDTD simulations. This allowed us to reduce the size of the simulation domain to a smaller volume surrounding the micro-lens.

In Fig. 2, the FWHM spot size is found by fitting a 2D Gaussian function to the z component of the Poynting vector at the plane of focus (shown in Fig. 2c). The focusing efficiency is defined as the fraction of the incident light that passes through a circular aperture in the plane of focus with a radius equal to three times the FWHM spot size.

References

1. Stork, W., Streibl, N., Haidner, H. & Kipfer, P. Artificial distributed-index media fabricated by zero-order gratings. *Opt. Lett.* **16,** 1921–1923 (1991).
2. Chen, F. T. & Craighead, H. G. Diffractive phase elements based on two-dimensional artificial dielectrics. *Opt. Lett.* **20,** 121–123 (1995).
3. Warren, M. E., Smith, R. E., Vawter, G. A. & Wendt, J. R. High-efficiency subwavelength diffractive optical element in GaAs for 975 nm. *Opt. Lett.* **20,** 1441–1443 (1995).
4. Chen, F. T. & Craighead, H. G. Diffractive lens fabricated with mostly zeroth-order gratings. *Opt. Lett.* **21,** 177–179 (1996).
5. Lalanne, P., Astilean, S., Chavel, P., Cambril, E. & Launois, H. Blazed binary subwavelength gratings with efficiencies larger than those of conventional échelette gratings. *Opt. Lett.* **23,** 1081–1083 (1998).
6. Verslegers, L. *et al.* Planar lenses based on nanoscale slit arrays in a metallic film. *Nano Lett.* **9,** 235–238 (2009).
7. Yu, N. *et al.* Light propagation with phase discontinuities: generalized laws of reflection and refraction. *Science* **334,** 333–337 (2011).
8. Kildishev, A. V., Boltasseva, A. & Shalaev, V. M. Planar photonics with metasurfaces. *Science* **339,** 1232009 (2013).
9. Yu, N. & Capasso, F. Flat optics with designer metasurfaces. *Nat. Mater.* **13,** 139–150 (2014).
10. Huang, F. M., Kao, T. S., Fedotov, V. A., Chen, Y. & Zheludev, N. I. Nanohole array as a lens. *Nano Lett.* **8,** 2469–2472 (2008).
11. Aieta, F. *et al.* Aberration-free ultrathin flat lenses and axicons at telecom wavelengths based on plasmonic metasurfaces. *Nano Lett.* **12,** 4932–4936 (2012).
12. Ni, X., Ishii, S., Kildishev, A. V. & Shalaev, V. M. Ultra-thin, planar, Babinet-inverted plasmonic metalenses. *Light Sci. Appl.* **2,** e72 (2013).
13. Genevet, P. *et al.* Ultra-thin plasmonic optical vortex plate based on phase discontinuities. *Appl. Phys. Lett.* **100,** 013101 (2012).
14. Karimi, E. *et al.* Generating optical orbital angular momentum at visible wavelengths using a plasmonic metasurface. *Light Sci. Appl.* **3,** e167 (2014).
15. Monticone, F., Estakhri, N. M. & Alù, A. Full control of nanoscale optical transmission with a composite metascreen. *Phys. Rev. Lett.* **110,** 203903 (2013).
16. Arbabi, A. & Faraon, A. Fundamental limits of ultrathin metasurfaces. Preprint at http://arxiv.org/abs/1411.2537 (2014).
17. Chen, L., Huang, M. C. Y., Mateus, C. F. R., Chang-Hasnain, C. J. & Suzuki, Y. Fabrication and design of an integrable subwavelength ultrabroadband dielectric mirror. *Appl. Phys. Lett.* **88,** 031102 (2006).
18. Kemiktarak, U., Metcalfe, M., Durand, M. & Lawall, J. Mechanically compliant grating reflectors for optomechanics. *Appl. Phys. Lett.* **100,** 061124 (2012).
19. Wu, T. T. *et al.* Sub-wavelength GaN-based membrane high contrast grating reflectors. *Opt. Express* **20,** 20551–20557 (2012).
20. Mateus, C., Huang, M., Deng, Y., Neureuther, A. & Chang-Hasnain, C. Ultrabroadband mirror using low-index cladded subwavelength grating. *IEEE Photon. Technol. Lett.* **16,** 518–520 (2004).
21. Lu, F., Sedgwick, F. G., Karagodsky, V., Chase, C. & Chang-Hasnain, C. J. Planar high-numerical-aperture low-loss focusing reflectors and lenses using subwavelength high contrast gratings. *Opt. Express* **18,** 12606–12614 (2010).
22. Astilean, S., Lalanne, P., Chavel, P., Cambril, E. & Launois, H. High-efficiency subwavelength diffractive element patterned in a high-refractive-index material for 633 nm. *Opt. Lett.* **23,** 552–554 (1998).
23. Fattal, D., Li, J., Peng, Z., Fiorentino, M. & Beausoleil, R. G. Flat dielectric grating reflectors with focusing abilities. *Nat. Photonics* **4,** 466–470 (2010).
24. Klemm, A. B. *et al.* Experimental high numerical aperture focusing with high contrast gratings. *Opt. Lett.* **38,** 3410–3413 (2013).
25. Lin, D., Fan, P., Hasman, E. & Brongersma, M. L. Dielectric gradient metasurface optical elements. *Science* **345,** 298–302 (2014).
26. Arbabi, A. *et al.* Controlling the phase front of optical fiber beams using high contrast metastructures - OSA Technical Digest (online). In *CLEO: 2014.* STu3M.4 Optical Society of America, 2014; Available at http://www.opticsinfobase.org/abstract.cfm?URI=CLEO_SI-2014-STu3M.4.
27. Vo, S. *et al.* Sub-wavelength grating lenses with a twist. *IEEE Photon. Technol. Lett.* **26,** 1375–1378 (2014).
28. Shiono, T., Kitagawa, M., Setsune, K. & Mitsuyu, T. Reflection micro-Fresnel lenses and their use in an integrated focus sensor. *Appl. Opt.* **28,** 3434–3442 (1989).
29. Haruna, M., Takahashi, M., Wakahayashi, K. & Nishihara, H. Laser beam lithographed micro-Fresnel lenses. *Appl. Opt.* **29,** 5120–5126 (1990).
30. Staude, I. *et al.* Tailoring directional scattering through magnetic and electric resonances in subwavelength silicon nanodisks. *ACS Nano* **7,** 7824–7832 (2013).
31. Decker, M. *et al.*High-efficiency light-wave control with all- dielectric optical Huygens' metasurfaces. Preprint at http://arxiv.org/abs/1405.5038 (2014).
32. Oskooi, A. F. *et al.* Meep: A flexible free-software package for electromagnetic simulations by the FDTD method. *Comput. Phys. Commun.* **181,** 687–702 (2010).
33. Arbabi, A., Horie, Y. & Faraon, A. Planar retroreflector - OSA Technical Digest (online). In *CLEO: 2014.* STu3M.5 Optical Society of America, 2014; Available at http://www.opticsinfobase.org/abstract.cfm?URI=CLEO_SI-2014-STu3M.5.

Acknowledgements

This work was supported by the Caltech/JPL president and director fund (PDF). A.A. was also supported by DARPA. Y.H. was supported by the JASSO fellowship and the 'Light-Material Interactions in Energy Conversion' Energy Frontier Research Center funded by the US Department of Energy, Office of Science, Office of Basic Energy Sciences under Award no. DE-SC0001293. Alexander Ball was supported by the Summer Undergraduate Research Fellowship (SURF) at Caltech. The device nanofabrication was performed in the Kavli Nanoscience Institute at Caltech. We thank David Fattal and Sonny Vo for useful discussion.

Author contributions

A.A., M.B. and A.F. conceived the experiment. A.A. and A.J.B. performed the FDTD simulations. A.A., Y.H. and M.B. fabricated the samples. A.A. performed the measurements, and analysed the data. A.A. and A.F. wrote the manuscript with input from all authors.

Additional information

Supplementary Information accompanies this paper at http://www.nature.com/naturecommunications

Competing financial interests: The authors declare no competing financial interests.

Reprints and permission information is available at http://npg.nature.com/reprintsandpermissions/

How to cite this article: Arbabi, A. *et al.* Subwavelength-thick lenses with high numerical apertures and large efficiency based on high-contrast transmitarrays. *Nat. Commun.* 6:7069 doi: 10.1038/ncomms8069 (2015).